International Journal of Engineering and Technology Innovation, vol. 16, no. 3, 2026, pp. 414-432

Balancing Curtailment and Economy in Source-Load Dispatch and Operation Management Systems Using DC-OPF and NSGA-II

Yang Zhang*, Weinan Zheng, Han Zheng, Zhuang Dou, Jun Shi

Shenzhen Power Supply Bureau Co., Ltd. of China Southern Power Grid, Guangdong, Shenzhen, 518001, China

Received 05 April 2026; revised 01 July 2026; accepted 10 July 2026

DOI: https://doi.org/10.46604/ijeti.2026.16343

Abstract

Integrating high shares of renewable energy requires dispatch tools that minimize operating cost and renewable curtailment while respecting network constraints. This study develops a transmission-aware source-load dispatch framework based on lossless DC optimal power flow (DC-OPF). A deterministic 24-hour scheduling case is constructed using a modified IEEE 30-bus system. Renewable utilization and curtailment are explicitly incorporated as decision variables. The model minimizes operating cost and renewable curtailment subject to network and operating constraints. Under the same input data and renewable accounting scheme, its performance is compared with a network-unconstrained economic dispatch baseline and a bi-objective NSGA-II approach. Results show that DC-OPF limits renewable curtailment to 0.03 MWh while increasing operating cost by only 0.41% relative to the unconstrained baseline. The selected NSGA-II solution remains approximately 4% more expensive. The results indicate that transmission-aware dispatch can achieve near-complete renewable utilization with a marginal economic penalty under the tested operating conditions.

Keywords: DC optimal power flow, NSGA-II, renewable curtailment, economic dispatch, new energy management system

1. Introduction

The increasing emphasis on achieving low carbon electricity systems has increased the importance of renewable energy adoption. Although these resources achieve the desired objectives of reduced reliance on fuel and lower emissions, their intermittency and lack of controllability complicate their short-term dispatch [1, 2]. The central challenge in practical power systems is not only to minimize thermal generation, but also to maintain system feasibility under generator limits and transmission constraints while balancing renewable availability.

Classical economic dispatch solves a cost minimization problem subject to power balance and generator operating limits [3]. Although it is computationally efficient and still a standard benchmark, it does not represent the transmission network explicitly or reveal how economic performance varies when renewable curtailment is treated as a separate entity in the operational objective. On the other hand, optimal power flow embeds network equations along with operating limits directly into the optimization model [4]. DC optimal power flow (DC-OPF) is especially attractive in the day-ahead scheduling studies because it preserves tractability while also representing active power balance and line flow constraints within the limits of acceptable frequency for a range of transmission-level applications [5].

Nevertheless, the practical value of advanced multi-objective optimization depends strongly on the operating regime being studied. In many transmission-level scheduling problems, DC optimal power flow captures the essential balance between economy and network feasibility with sufficient clarity for operational decision-making [6]. For this reason, the present study centers the analysis on DC-OPF and uses NSGA-II as a secondary exploratory tool to examine whether the tested system

* Corresponding author. E-mail address: zhengwn316@163.com

exhibits a meaningful trade-off between operating cost and renewable curtailment. This comparison helps distinguish cases in which transmission-aware cost minimization is already sufficient from those in which Pareto-based search offers additional decision-making value [4].

NSGA-II and other Pareto-based methods have been extensively used in economic and environmental dispatch problems in power systems. Abido [7] demonstrated the effectiveness of Pareto ranking for dispatch problems that have competing objectives. Later, studies extended this work into more complex generator models with dynamic dispatch and tighter constraint handling. Nourianfar et al. [8] reported improved performance for combined heat and power dispatch applications by employing a hybrid NSGA-II and MOPSO strategy. Some recent studies continue this trend and confirm that the non-dominated search remains competitive in the domain of multi-objective dispatch and OPF under highly non-linear feasible spaces [9, 10].

There is also a second stream of research that focuses on OPF with the inclusion of stochastic renewable generation. Bhavsar et al. [11] introduced an influential economic dispatch model that accounts for the uncertainty of wind power. Ali et al. [12] then showed that uncertainty in renewable generation, along with multi-objective search, is closely linked in OPF studies. Li et al. [13] and Maheshwari et al. [14] then demonstrated that solar and wind modeling materially change the optimal flow behavior on standard IEEE benchmark systems. These studies support the use of benchmark transmission networks with renewable injections when comparing solution quality across methods.

A third body of literature deals more explicitly with renewable curtailment. A well-known review by Bird et al. [15] indicated that the influence of curtailment is determined by bottlenecks in transmission, rigid thermal generation, operational reserve conditions, and market design. Recent research has looked at curtailment reduction through network reconfiguration, flexibility, and coordinated dispatch. Pijarski et al. [16] indicated the existence of a strong relationship between line overload management and curtailment reduction in renewable-rich networks. Flexibility due to demand response, storage, and transmission expansion was discussed in the study by Rahman et al. [2] and observed to become more relevant with the increasing renewable penetration. Laimon [17] further argued that curtailment should not only be viewed as an operational loss but also as an indicator of a lack of flexibility and adaptability in the network.

Source-load coordination has also drawn increasing interest because flexible demand can help reduce operating costs as well as the spillage of renewable energy. Ren et al. [18] examined the use of virtual power stations under source-load uncertainty and indicated that coordinated scheduling enhances renewable accommodation. Zhang et al. [17] showed that flexible load response can enhance economic dispatch performance in the presence of wind power. Similar results were also found by Li et al. [19] in load systems, where the coordinated scheduling increased the utilization of renewables under uncertainty and network risk. Taken together, these studies encourage source-load dispatch formulations that do not lose sight of either the supply side or the flexibility side.

Another related theme is benchmark modeling practice. To date, MATPOWER and the IEEE 30-bus system remain standard research tools for dispatch and OPF validation because of their transparent data structures and reproducible test cases [20]. The recent OPF surveys and reviews also stressed that the algorithms comparisons must differentiate between the cases of unconstrained economic scheduling, the network-constrained OPF, and the genuinely multi-objective formulations [21]. This distinction is significant since differences in constraint formulations may influence solution quality as much as optimization algorithms.

Although the field is quite mature, some wide gaps remain that are quite relevant to this study. The first gap is that many studies place heavy emphasis on metaheuristics, but they do not compare them carefully against an explicit transmission-aware baseline on the same 24-hour data set [21]. The second gap is that the renewable curtailment is often discussed qualitatively, but the mathematical treatment of utilization of renewables, their curtailment, and thermal-limits thresholds is not fully presented in a consistent manner [16]. Another gap is the dearth of studies that translate algorithmic results into practical operating insights regarding whether network constraints impose a material economic premium under moderate renewable penetration. This paper addresses these gaps through the following contributions:

(1) It formulates a consistent 24-hour source-load dispatch model in which renewable utilization and renewable curtailment are represented explicitly through renewable utilization variables.
(2) It benchmarks a transmission-aware DC-OPF formulation against an unconstrained economic baseline and an NSGA-II-based multi-objective formulation under the same generator data, load profile and renewable profile.
(3) It shows, for the studied modified IEEE 30-bus system, that network-feasible dispatch can achieve near-zero renewable curtailment with only a small economic premium relative to the unconstrained baseline.
(4) It clarifies the operating conditions under which multi-objective search provides additional insight beyond DC-OPF, particularly when renewable penetration, generator operating limits and network congestion create a stronger economic-physical conflict.

It should be noted that the novelty of this work lies not in the optimiser but in how renewable curtailment is represented and exploited within the dispatch problem itself. The difference lies in how renewable energy is treated inside the dispatch. In most formulations, the renewable injection is fixed, and curtailment is obtained by subtracting the dispatched renewable power from the available power after optimization. In the model proposed here, the utilized renewable power and the curtailed power are both retained as decision variables, tied to the available power by an equality constraint that forms part of the feasible region. Since this constraint sits within the optimization, the level of curtailment is set by the solver rather than measured afterwards; when the network cannot accommodate the full renewable output, only as much is curtailed as is needed to keep the schedule feasible at minimum cost.

The same renewable variables and the same coupling constraint are used in the unconstrained baseline and in the NSGA-II model as well. The cost and curtailment values reported for the three methods therefore come from one common accounting scheme, and the differences between them reflect the constraint set imposed on each method rather than any difference in how the renewable energy was quantified.

Beyond this modelling choice, the study contributes a controlled comparison of the three methods on a single 24-hour dataset. It also provides a quantitative map of the operating conditions, namely penetration, transmission headroom, and single-line outages, under which the network premium and the curtailment move from negligible to significant.

This contribution addresses an important gap in the literature, where OPF and metaheuristic results are often reported without first establishing whether the network actually limits the dispatch, and therefore without showing whether multi-objective search is warranted. The original NSGA-II of Deb et al. [22] and recent multi-objective OPF studies [23-25] are taken as the methodological basis for this part of the work.

The remainder of the paper is organized as follows. Section 2 presents the mathematical problem formulation. Section 3 describes the implementation of DC-OPF, NSGA-II and the baseline. Section 4 introduces the IEEE 30-bus case study. Section 5 reports and discusses the results. Section VI concludes the paper.

2. Problem Formulation

2.1 System Model and Decision Variables

Consider a power system operated over a scheduling horizon of T hourly intervals with N_g dispatchable thermal units and time-varying renewable availability from wind and solar sources. The thermal dispatch decision is denoted by $P_{g,i,t}$, which represents the real power output of generator i at hour t. To explicitly couple renewable scheduling and curtailment within the optimization model, the utilized renewable power is represented by R_t^{used}, bounded by the available renewable power R_t^{avail}. In addition, a curtailment slack variable C_t is retained so that the renewable accounting relation becomes part of the optimization model rather than only a post-processing definition. The decision vector is therefore written as:

$$\mathbf{x} = \left\{P_{g,i,t}, R_t^{\text{used}}, C_t\right\}_{i=1,\ldots,N_g;\, t=1,\ldots,T} \tag{1}$$

For the 24-hour, six-generator case studied here, the thermal dispatch component contains 6 × 24 = 144 continuous variables. In the DC-OPF benchmark, bus voltage angles are introduced as auxiliary state variables to enforce network feasibility. This formulation remains close to the original source-load model while making renewable scheduling more explicit and easier to interpret in a multi-objective setting.

2.2 Objective Functions

The optimization problem is posed as a bi-objective minimization problem:

$$\min_{\mathbf{x}\in\Omega} \ \mathbf{F}(\mathbf{x}) = \left[f_1(\mathbf{x}), f_2(\mathbf{x})\right] \tag{2}$$

where Ω denotes the feasible set induced by the operating constraints, f_1 is the total thermal operating cost, and f_2 is the total renewable curtailment.

The feasible set in Eq. (2) is defined by the set of all dispatch and renewable schedules that satisfy, at every hour, the power-balance equality, generator output limits, directional ramp limits, renewable utilization bounds, and the curtailment coupling. In the DC-OPF benchmark, it also contains the nodal-balance relation and the line-flow limits. A schedule is considered feasible only when all constraints are simultaneously satisfied; otherwise, it is excluded from the comparison.

Objective 1 Total Operating Cost

The hourly fuel cost of generator i is represented by the standard quadratic cost function:

$$c_i(P_{g,i,t}) = a_i + b_i P_{g,i,t} + c_i P_{g,i,t}^2 \tag{3}$$

where a_i, b_i, and c_i are generator cost coefficients. To keep the model close to the original formulation while improving its time-coupled character, the operating cost may be written in augmented form as:

$$f_1(\mathbf{x}) = \sum_{t=1}^{T}\sum_{i=1}^{N_g}\left[c_i\left(P_{g,i,t}\right) + \lambda_i\left(P_{g,i,t} - P_{g,i,t-1}\right)^2\right] \tag{4}$$

where $\lambda_i \geq 0$ is a small ramp-smoothing coefficient. When $\lambda_i = 0$, Eq. (4) reduces exactly to the original objective. The second term is introduced only to make the formulation more flexible and to penalize unnecessary inter-hour dispatch oscillations, which is conceptually aligned with dynamic scheduling practice in the literature [21].

Objective 2 Total Renewable Curtailment

Renewable curtailment at hour t is defined as the difference between available and utilized renewable power:

$$C_t = R_t^{\text{avail}} - R_t^{\text{used}} \tag{5}$$

subject to

$$0 \leq R_t^{\text{used}} \leq R_t^{\text{avail}} \quad \forall t \tag{6}$$

and

$$C_t \geq 0 \quad \forall t \tag{7}$$

To keep the renewable accounting relation fully embedded within the feasible set, Eq. (5) is enforced directly rather than treated only as a derived quantity. This is consistent with curtailment modeling practice where available renewable energy is partitioned into utilized and curtailed components [17]. The cumulative curtailment objective is written as:

$$f_2(\mathbf{x}) = \sum_{t=1}^{T} \omega_t C_t \tag{8}$$

where $\omega_t \geq 0$ is a time-dependent weighting factor. In the base case, $\omega_t = 0$ for all t, which recovers the original formulation exactly. The weighted form is retained because it offers a more general and alternative representation, allowing selected hours with system stress or high renewable availability to be emphasized without changing the overall structure of the model.

Two quantities are optimized explicitly: the operating cost and the total curtailment. Load balancing and reliability are not separate objectives here; they enter as hard constraints. Load balancing is the hourly power-balance equality, while reliability is represented by the generator limits, the ramp limits, and the transmission limits, supported by an installed thermal capacity of 485 MW against a peak demand of 286.8 MW, which leaves a reserve in every hour. Keeping the objective vector two-dimensional is what makes the Pareto results in Section 5 interpretable.

2.3 Constraints

Power Balance Equality Constraint

At each hour, dispatched thermal generation plus utilized renewable generation must satisfy total demand:

$$\sum_{i=1}^{N_g} P_{g,i,t} + R_t^{\text{used}} = P_{\text{load},t} \quad \forall t \tag{9}$$

Transmission losses are neglected in the base formulation, consistent with the DC approximation adopted for the network-constrained benchmark [26]. To facilitate implementation, the balance mismatch can also be written in residual form as:

$$\varepsilon_t^{\text{bal}} = \sum_{i=1}^{N_g} P_{g,i,t} + R_t^{\text{used}} - P_{\text{load},t} = 0 \quad \forall t \tag{10}$$

Generator Capacity Limits

Each thermal unit must operate within its minimum and maximum output limits:

$$P_{g,i}^{\min} \leq P_{g,i,t} \leq P_{g,i}^{\max} \quad \forall i, t \tag{11}$$

These limits define the local feasible dispatch interval of each thermal unit and remain unchanged from the original model.

Ramp-Rate Constraints

Inter-temporal ramping limits are imposed to avoid unrealistic changes in thermal output. In place of a single symmetric absolute-value statement, the constraint is written in directional form as:

$$-\Delta P_{g,i}^{\text{down}} \leq P_{g,i,t} - P_{g,i,t-1} \leq \Delta P_{g,i}^{\text{up}}, \forall i, t = 2, \ldots, T \tag{12}$$

where $\Delta P_{g,i}^{\text{up}}$ and $\Delta P_{g,i}^{\text{down}}$ denote the ramp-up and ramp-down limits of unit *i*. If symmetric ramps are assumed, then $\Delta P_{g,i}^{\text{up}} = \Delta P_{g,i}^{\text{down}} = \Delta P_{g,i}^{\text{ramp}}$ and Eq. (12) reduces to the original ramp-rate model. This form provides greater modeling fidelity and is closer to practical generator scheduling constraints used in dispatch studies.

Renewable Feasibility Coupling

To strengthen the renewable part of the model without changing its basic logic, the utilized renewable power and curtailment are linked through the explicit feasibility relation:

$$R_t^{\text{used}} + C_t = R_t^{\text{avail}} \quad \forall t \tag{13}$$

This equation is mathematically equivalent to Eq. (5), but it is useful to state it directly because it turns renewable accounting into an equality constraint which will be easier for the optimization engine to handle.

Transmission Line Flow Constraints in DC-OPF

Active power flow on line ℓ connecting buses *m* and *n* is modeled as:

$$f_{\ell,t} = \frac{\theta_{m,t} - \theta_{n,t}}{x_\ell} \tag{14}$$

where $\theta_{m,t}$ is the bus voltage angle and x_l is the series reactance of the line. The corresponding thermal limit is:

$$-F_\ell^{\max} \le f_{\ell,t} \le F_\ell^{\max} \quad \forall \ell, t \tag{15}$$

To express the network model in compact form, the DC power balance can also be written in compact nodal form as:

$$\mathbf{B}_{\text{bus}} \boldsymbol{\theta}_t = \mathbf{P}_t^{\text{inj}} \tag{16}$$

where $\mathbf{B}_{bus}$ is the bus susceptance matrix and $\mathbf{P}_t^{\text{inj}}$ is the nodal net injection vector at hour t. This compact relation does not replace the original line-flow equations. Instead, it clarifies the network structure that underlies the benchmark and makes the formulation more consistent.

The DC-OPF benchmark adopts the standard linearization assumptions. Voltage magnitudes are held at one per unit, reactive power and shunt effects are not modeled, and resistive losses are neglected. These assumptions are conventional for transmission-level day-ahead screening and are accepted here because the comparison concerns active-power redispatch and curtailment, not voltage support. The consequence of these assumptions is that losses and voltage limits are not captured, so the premiums reported later are lower bounds on what an AC model would give; an AC-OPF check is left to future work.

Constraint Violation Measure

Let the aggregate violation measure be:

$$\text{CV}(\mathbf{x}) = \sum_{t=1}^{T} \left| \varepsilon_t^{\text{bal}} \right| + \sum_{i=1}^{N_g} \sum_{t=1}^{T} \Gamma_{i,t}^{\text{cap}} + \sum_{i=1}^{N_g} \sum_{t=2}^{T} \Gamma_{i,t}^{\text{ramp}} + \sum_{t=1}^{T} \Gamma_t^{\text{ren}} \tag{17}$$

where

$$\Gamma_{i,t}^{\text{cap}} = \max\left(0, P_{g,i}^{\min} - P_{g,i,t}\right) + \max\left(0, P_{g,i,t} - P_{g,i}^{\max}\right) \tag{18}$$

$$\Gamma_{i,t}^{\text{ramp}} = \max\left(0, P_{g,i,t} - P_{g,i,t-1} - \Delta P_{g,i}^{\text{up}}\right) + \max\left(0, P_{g,i,t-1} - P_{g,i,t} - \Delta P_{g,i}^{\text{down}}\right) \tag{19}$$

and

$$\Gamma_t^{\text{ren}} = \left| R_t^{\text{used}} + C_t - R_t^{\text{avail}} \right| \tag{20}$$

Concretely, the aggregate violation is the sum of the non-negative parts of all inequality constraints, each written in the less-than-or-equal-to-zero form. For the present model, these are the two power-balance inequalities per hour, the generator-bound violations, the directional ramp violations, and, in the DC-OPF case, the line-flow violations. A candidate is feasible when this sum is zero, and any feasible candidate is preferred to any infeasible one.

Problem Size and Constraint Structure

Combining the time-coupled generator constraints with hourly power balance requirements results in a moderately sized constrained scheduling problem. For the case of 24 hours, the thermal dispatch component has 144 primary decision variables along with 24 power balance equations, and it also has 144 bound constraints on generator output and 138 ramp-rate inequalities. The explicit renewable representation further adds 24 utilized renewable variables along with 24 curtailment variables and their associated coupling constraints. This scale is sufficient to evaluate the optimization quality and modeling consistency without obscuring the comparison through an excessively large system size.

3. Methodology

Three dispatch strategies are implemented and compared, with DC-OPF serving as the primary transmission-aware benchmark and NSGA-II included as a complementary multi-objective comparator. Fig. 1 shows the detailed flowchart for the implemented DC-OPF framework.

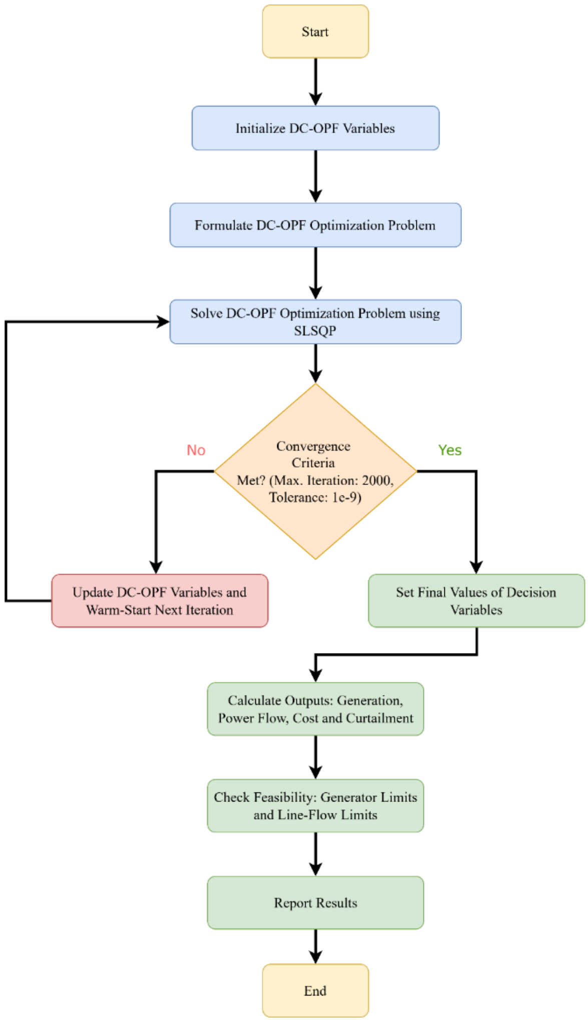

Fig. 1 Flowchart of the proposed DC-OPF framework

3.1 NSGA-II Multi-Objective Dispatch

NSGA-II maintains a population $\mathcal{P}$ of candidate schedules, each encoding the 24-hour thermal dispatch trajectory and the associated renewable utilization schedules. Feasible initial candidates are generated by balancing hourly demand against available renewable output and then allocating the residual net load among thermal generators within their operating limits. Repair steps are applied when necessary, so that the initial population satisfies the hourly balance equation and generator bounds. Each candidate is evaluated using the two objectives in Eq. (4) and Eq. (8). Constraint handling is based on total constraint violation:

$$\mathrm{CV}(\mathbf{x}_k) = \sum_j \max\left(0, g_j(\mathbf{x}_k)\right) \tag{21}$$

where $g_j(\cdot)$ denotes the *j*-th inequality constraint. Individuals with lower constraint violation are preferred, and fully feasible solutions dominate infeasible ones under the standard superiority-of-feasibility principle often used in constrained evolutionary optimization [12]. After objective evaluation, the combined parent and offspring population is sorted into non-dominated fronts. For two feasible solutions x_a and x_b, x_a is said to dominate x_b if it is no worse than x_b in all objectives and strictly better in at least one objective:

$$x_a \prec x_b \Leftrightarrow \left[f_k\left(x_a\right) \le f_k\left(x_b\right), \forall k \in \{1,\ldots,M\} \right] \wedge \left[\exists k \in \{1,\ldots,M\} : f_k\left(x_a\right) < f_k\left(x_b\right) \right] \tag{22}$$

Crowding distance is then used to preserve diversity along the non-dominated set,

$$d_k = \sum_{m=1}^{M} \frac{f_m(\mathbf{x}_{k+1}) - f_m(\mathbf{x}_{k-1})}{f_m^{\max} - f_m^{\min}} \tag{23}$$

where $M = 2$ for the present problem. Binary tournament selection, simulated binary crossover, and polynomial mutation are employed in the usual NSGA-II manner [6]. The implementation uses a population size of $N = 100$, crossover probability $p_c = 0.9$, polynomial mutation probability $p_m = 1/n_{\text{var}}$, and 50 generations for the comparison study.

The control parameters are summarized as follows. The population size is set to 100 and the comparison run uses 50 generations, while a longer 200-generation setting is adopted for the convergence study in Section V. Recombination is simulated using binary crossover with probability 0.9 and distribution index 15; mutation is polynomial with probability one over the number of variables (about 0.007) and distribution index 20; parents are chosen by binary tournament under the constrained-domination rule; and survival is the elitist plus-selection of the merged parent and offspring populations, ranked by non-dominated front and then by crowding distance. The initial population is feasibility-guided, and duplicates are removed. Thirty random seeds are used so that the outcome can be reported statistically rather than relying on a single run [22].

When a single schedule is selected from the non-dominated set for the tables, the best-compromise rule is applied: each objective is min-max normalised over the final front, and the solution with the smallest Euclidean distance to the ideal point is chosen. The size of the non-dominated set and the full front are reported in Section 5 so that this selection can be checked.

The cost of one generation is dominated by non-dominated sorting, which is of order M times N squared for a population N and M objectives, with the evaluation of the 144 decision variables adding a linear term and the memory being of order N squared. With a population of 100, this gives the run-times reported in Section 5, of the order of a second for 50 generations and a few seconds for 200, whereas the deterministic DC-OPF solves twenty-four small quadratic programs in well under a second; it is this gap that grows on larger systems.

NSGA-II is benchmarked against two references that bracket the achievable performance: a gradient-based weighted-sum and epsilon-constraint solver, which returns the exact deterministic front for this convex sub-problem, and the network-blind economic baseline. Placing the metaheuristic between a deterministic solver and a baseline is more informative for a transmission-aware study than exchanging one metaheuristic for another. Comparison with other population-based methods under stressed and non-convex instances is left for future work [23].

3.2 DC Optimal Power Flow

The DC-OPF benchmark minimises the total operating cost subject to power balance, generator limits, ramp-rate limits and line flow constraints. At each hour, the voltage angle vector $\boldsymbol{\theta}_t$ satisfies:

$$\mathbf{B}\boldsymbol{\theta}_t = \mathbf{P}_t^{\text{inj}} \tag{24}$$

where $\mathbf{B}$ is the DC susceptance matrix and $\mathbf{P}_t^{\text{inj}}$ is the vector of net active power injections. The model follows standard DC-OPF practice and serves as the transmission-aware benchmark for economic scheduling [5]. In the implementation adopted in this study, the hourly problem is solved sequentially using SLSQP and warm-started from the previous hour.

In this network model, the reference (slack) bus angle is fixed at zero at every hour, taken at bus 1, and the other bus angles are solved relative to it. The susceptance matrix appearing in the nodal relation is therefore the reduced matrix obtained after removing the reference row and column, which keeps the angle reference well defined.

This hour-by-hour solve does not conflict with the ramp-rate constraints. The hours are linked in a single forward pass: when hour t is solved, each generator is bounded by the interval set by its output at hour t minus one and its ramp-up and ramp-down limits. The previous solution is used as the warm start. The schedule is therefore coupled in time through the ramp bounds, even though the solver is called once per hour rather than on the whole 24-hour block at once.

3.3 Unconstrained Economic Baseline

The baseline provides a cost-oriented reference without explicit line flow constraints. To preserve comparability with the bi objective formulation, a weighted-sum scalarisation is used:

$$\min_{\mathbf{x}}\ w_1 \hat{f}_1(\mathbf{x}) + w_2 \hat{f}_2(\mathbf{x}) \tag{25}$$

where $\hat{f}_1$ and $\hat{f}_2$ are normalized objective values. Five weight combinations are explored, namely (0, 1), (0.25, 0.75), (0.5,0.5), (0.75, 0.25), and (1, 0). This baseline does not recover the full Pareto geometry, but it offers a simple reference for understanding the incremental value of non-dominated search.

In the weighted-sum reference, each objective is first divided by its own range, so that the normalised cost and normalised curtailment are dimensionless and lie on comparable scales; the weights are therefore unitless and sum to one. The ranges are taken from the single-objective cost and curtailment minima reported in Section 5. All three methods are evaluated under the same conditions, and the comparison is performed using operating cost, renewable curtailment, and congestion premium.

4. Case Study of the Modified IEEE 30-Bus System

4.1 Network Description

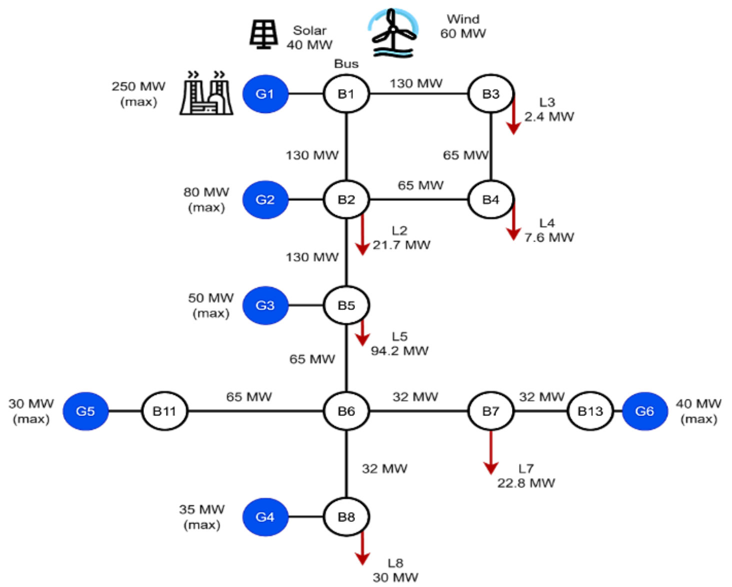

Fig. 2 Reduced network representation of the modified IEEE 30-bus system used in the study

The study uses a modified version of the IEEE 30-bus system, which is extensively used for economic dispatch and optimal power flow studies in the literature [27]. The original system contains 30 buses, 41 transmission branches, and six generators. In the present case, the scheduling study focuses on ten monitored transmission corridors that represent the most relevant thermal constraints for the simplified DC network model. The adopted topology is shown in Fig. 2.

4.2 Generator Parameters

Six thermal generating units are modelled with quadratic cost curves, ramp-rate limits and minimum up/down times. Table 1 summarises the generator parameters. The total installed conventional capacity is 485 MW, substantially exceeding the peak load of 286.8 MW to provide scheduling feasibility across all operating conditions. The monitored transmission lines are also given in Table 2.

Table 1 Thermal generator parameters

Gen.	Bus	$\mathbf{P}^{min}$(MW)	$\mathbf{P}^{max}$(MW)	$\mathbf{b}_i$($/MWh)	$\mathbf{c}_i$($/MW^{2}h)	$\mathbf{\Delta P}^{ramp}$ (MW/h)
G1	1	50	250	2.000	0.00375	100
G2	2	20	80	1.750	0.01750	40
G3	5	15	50	1.000	0.06250	25
G4	8	10	35	3.250	0.00834	17.5
G5	11	10	30	3.000	0.02500	15
G6	13	12	40	3.000	0.02500	20
Total		117	485	-	-	-

Table 2 Monitored transmission lines

Line	From-To	Reactance (p.u.)	Limit (MW)
L1	1-2	0.0575	130
L2	1-3	0.1852	130
L3	2-4	0.1763	65
L4	3-4	0.1719	130
L5	2-5	0.1998	130
L6	2-6	0.2998	65
L7	4-6	0.1700	90
L8	5-7	0.1400	70
L9	6-7	0.0920	130
L10	6-8	0.0919	32

4.3 Network Data and Reproducibility

The transmission checks use the reduced model that keeps the eight buses carrying the ten monitored corridors, Buses 1-8. The 60 MW wind plant and the 40 MW solar plant are connected at Bus 1. The six thermal units sit at buses 1, 2, 5, 8, 11 and 13; in the reduced network, the two units at buses 11 and 13 are electrically behind bus 8 and are mapped to that terminal. System demand is shared across the active buses following the standard IEEE 30-bus pattern, with the heaviest share at bus 5, and the shares are listed in Table A1 of the Appendix.

The constant cost term is zero for all six units and is therefore omitted from Table 1. The two coefficient columns correspond to the linear and quadratic terms of the quadratic fuel curve. These values are the standard normalized IEEE 30-bus coefficients, so the linear terms lie between 1.0 and 3.25 dollars per MWh rather than representing absolute fuel prices. With the generator data of Table 1, the line data of Table 2, the bus-load shares of Table A1, and the hourly load and renewable values of Table A2, the case is fully specified, and the reported results can be reproduced.

4.4 Renewable Energy Profiles

The renewable portfolio consists of a 60 MW wind plant and a 40 MW solar photovoltaic plant. The 24-hour profiles are intended to represent a moderate renewable integration scenario suitable for methodological comparison rather than site-specific forecasting. Solar output is zero during night hours, rises after sunrise, reaches a midday maximum near 40 MW, and declines toward evening. Wind output remains comparatively stable and ranges from approximately 29.9 MW to 45.0 MW over the day.

The combined renewable profile is shown in Fig. 3 together with the system load profile. Total renewable availability varies between 38.4 MW and 73.2 MW, while demand ranges from 174.7 MW to 286.8 MW. Accordingly, the net load remains positive in every hour, which means that thermal generation is required throughout the day. This operating pattern is useful for comparing redispatch behaviour across the three methods.

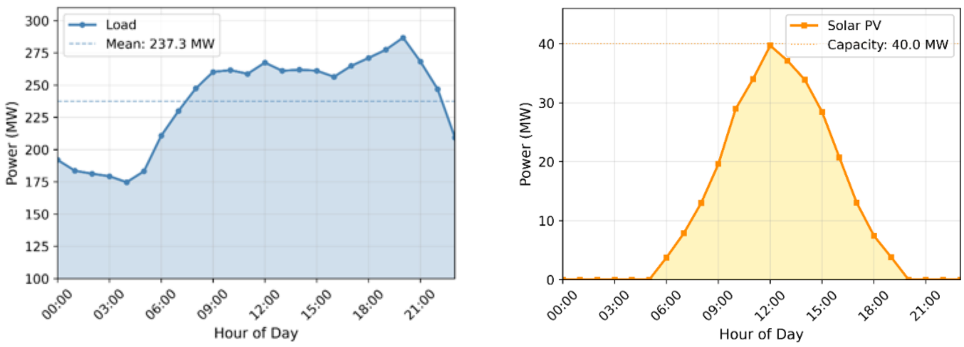

(a) System load profile (b) Solar PV generation profile

Fig. 3 24-hour system input profiles showing total load, solar PV generation, wind generation, and dispatch overview

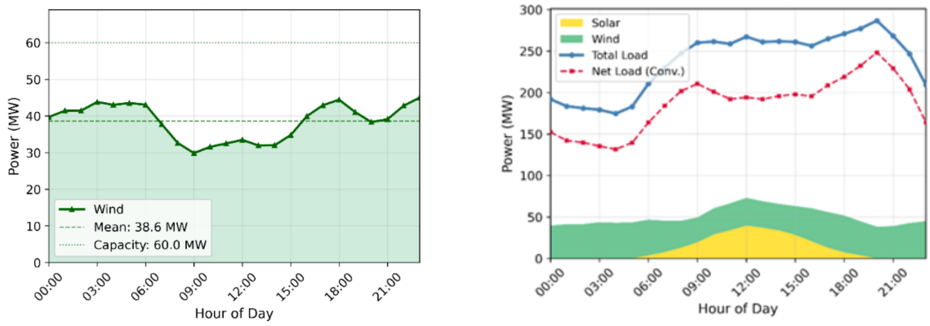

(c) Wind generation profile

(d) Dispatch overview (stacked)

Fig. 3 24-hour system input profiles showing total load, solar PV generation, wind generation, and dispatch overview (continued)

4.5 Problem Scale

The case study combines 24 hourly intervals, six thermal generators, and explicit renewable availability. The NSGA-II and baseline formulations optimise the multi-hour thermal dispatch while enforcing generator bounds, hourly power balance, renewable utilization bounds, and ramp-rate limits. The DC-OPF benchmark adds the auxiliary network variables and line flow constraints required for transmission feasibility.

5. Results and Discussion

5.1 Overall Performance Comparison

Table 4 reports the aggregate 24-hour metrics for the three dispatch strategies. The unconstrained baseline achieves the lowest cost, namely $11,282.26, because it does not enforce transmission limits. The DC-OPF solution increases the cost only modestly to $11,328.51 while maintaining renewable curtailment at 0.03 MWh. This corresponds to a congestion premium of 0.41%, which indicates that network feasibility can be achieved with only a small economic penalty in the studied configuration.

Table 3 24-Hour dispatch performance summary metrics

Method	Total Cost ($)	Curtailment (MWh)	Avg. Cost ($/MWh)	Congestion Premium
Unconstrained Baseline	11,282.26	0.00	1.921	-
NSGA-II	11,768.95	5.81	2.066	+$486.69
DC-OPF	11,328.51	0.03	1.989	+46.26 (0.41%)

The average-cost column in Table 3, close to 1.9 to 2.1 dollars per MWh, is the total operating cost divided by the energy served over the day. The level is low because the IEEE 30-bus cost curves used here are the standard normalized set, with linear coefficients between 1.0 and 3.25 dollars per MWh, rather than absolute fuel prices; what matters for the comparison is the difference between methods in this column, not its absolute value.

Table 4 24-Hour dispatch performance summary metrics

Method	Total Cost ($)	Curtailment (MWh)	Avg. Cost ($/MWh)	Congestion Premium
Unconstrained Baseline	11,282.26	0.00	1.921	-
NSGA-II	11,768.95	5.81	2.066	+$486.69
DC-OPF	11,328.51	0.03	1.989	+46.26 (0.41%)

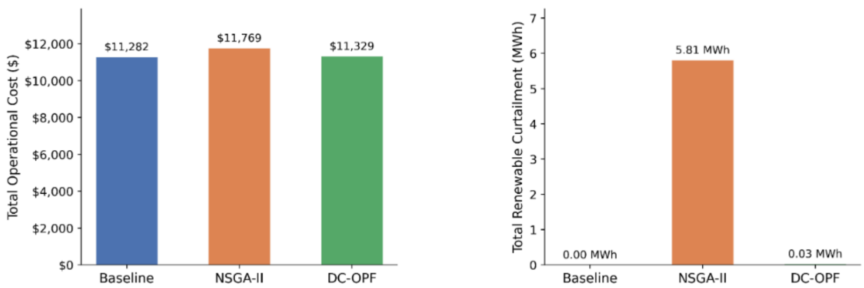

(a) Total 24-hour operational cost

(b) Total 24-hour renewable curtailment

Fig. 4 Comparative bar chart: total 24-hour operating cost and renewable curtailment

Fig. 4 provides a side-by-side visual comparison of total cost and curtailment across the three methods. The figure highlights that the DC-OPF method achieves near-zero curtailment while imposing an economically small congestion premium of 0.41%. This outcome is attributable to the relatively modest network loading in the 30-bus configuration under the tested generation mix, where maximum line utilization remains below 70% even during peak hours.

The selected NSGA-II solution has a total cost of $11,768.95 and renewable curtailment of 5.81 MWh. This outcome should be interpreted as one compromise solution drawn from the final non-dominated search rather than as the unique best schedule for cost minimization. That distinction is important because a multi-objective algorithm is designed to explore trade-offs, not to reproduce the single-objective cost optimum exactly.

5.2 Statistical Evaluation and Convergence of NSGA-II

Because NSGA-II is stochastic, it was run thirty times from independent random seeds at the 50-generation setting and repeated using a 200-generation setting. Table 5 reports the resulting statistics, and Fig. 5 shows the solution positions and the convergence of the search.

Table 5 NSGA-II performance over thirty independent runs

Setting	Cost mean ± std ($)	Best cost ($)	Curtailment mean ± std (MWh)	Run-time (s)	No. of solutions
NSGA-II, 50 generations	11,755.1 ± 1.1	11,751.7	6.45 ± 0.89	1.6	~81
NSGA-II, 200 generations	11,750.3 ± 1.4	11,745.6	5.81 ± 0.72	6.7	~24
Deterministic optimum	11,281.9	11,281.9	0.00	<1	1

The run-to-run spread is small, with a standard deviation near one dollar in cost and a few tenths of an MWh in curtailment, so the algorithm is repeatable. It is also clearly dominated: even at 200 generations, the best cost found, 11,745.6 dollars, is about 4.1% above the deterministic optimum of 11,281.9 dollars, while the curtailment of the deterministic and DC-OPF schedules is already close to zero. The 95% confidence interval on the mean cost is narrower than five dollars at both settings, so the gap to the deterministic optimum is far larger than the sampling noise. The single NSGA-II point listed in Table 4 is one run from this distribution.

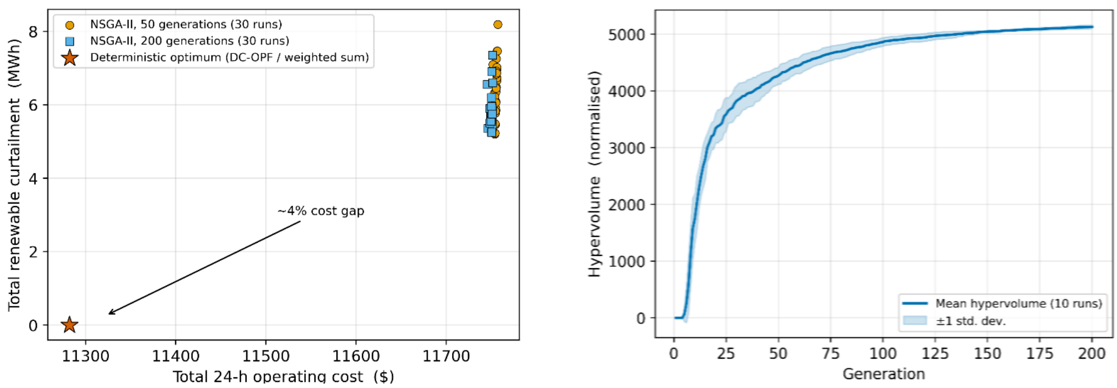

(a) Cost-curtailment distribution (b) Hypervolume convergence

Fig. 5 NSGA-II performance over thirty independent runs: (a) cost-curtailment distribution and (b) mean hypervolume convergence with one standard deviation

The hypervolume in Fig. 5(b) rises steeply over the first twenty to thirty generations and then flattens, so the search has settled well before 200 generations. The residual cost gap is therefore a property of the method on this smooth, almost convex problem and not a matter of stopping too early.

The non-dominated set itself is narrow. In the base case, the utilized renewable energy is absorbed by the network at almost no additional cost, so lower cost and lower curtailment are reached by the same low-thermal schedules, and the two objectives hardly conflict. The front collapses towards a single knee, which is the reason a multi-objective search returns little here that a single transmission-aware cost minimisation does not already provide.

5.3 Hourly Cost Profile Analysis

Fig. 6 shows the hourly generation cost profiles for all three methods across the 24-hour horizon. The cost curves exhibit a clear correlation with load demand: low costs during off-peak hours (00:00-06:00) when thermal generation is near its minimum operating levels, rising to peak costs during the evening ramp (19:00-21:00) when solar output is unavailable, and wind cannot fully offset load growth.

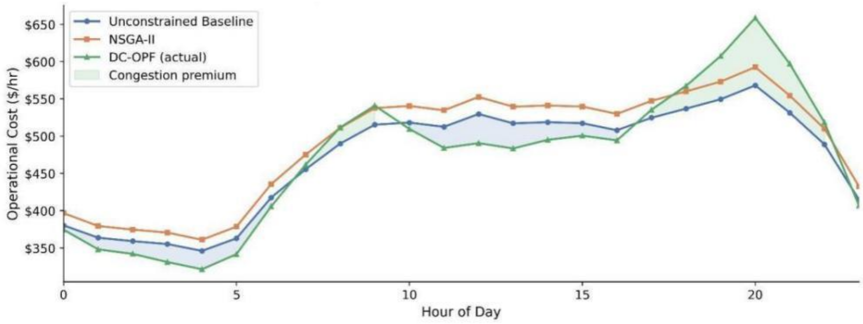

Fig. 6 Hourly operating cost profiles ($/h) for the three dispatch methods

The DC-OPF and baseline cost profiles are nearly indistinguishable for most hours, consistent with the aggregate congestion premium of only 0.41%. The most significant hourly divergence occurs during peak loading hours (hours 19-21), where transmission constraints redirect generation from lower-cost to higher-cost units to maintain line feasibility. The NSGA-II hourly costs exceed both comparators throughout the day, reflecting the higher total operating costs over the horizon.

5.4 Generation Dispatch Stack Analysis

Fig. 7 compares the 24-hour generation dispatch stacks for the unconstrained baseline and DC-OPF. Each stacked bar segment represents the contribution of individual generators and renewable sources to total system output at each hour.

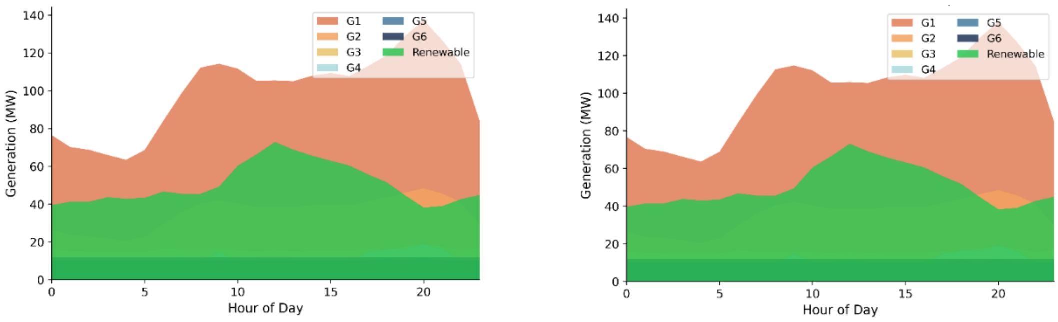

(a) Unconstrained baseline dispatch (scaled) (b) DC-OPF network-constrained dispatch

Fig. 7 24-hour generation dispatch stacks comparing (a) the unconstrained baseline and (b) the network-constrained DC-OPF solution

The baseline dispatch is dominated by G1 (the largest and moderately priced unit at $2.00/MWh linear coefficient) and G3 (the lowest marginal cost at $1.00/MWh linear coefficient), which together serve as the primary swing generators. Renewable resources are dispatched at full available output in all hours under the baseline, consistent with their zero marginal cost. The DC-OPF stack reveals subtle re-dispatching: G1 output is moderately reduced on certain high-load corridors, with G2 compensating to relieve thermal constraints on lines L1 (Bus 1-2) and L3 (Bus 2-4). This counter-flow adjustment accounts for the small congestion premium without materially altering the overall dispatch composition.

5.5 Transmission Line Loading Analysis

Fig. 8(a) presents the hourly line-loading heatmap, expressed as the percentage utilization of each line’s thermal limit across the 24-hour horizon. Figs. 8(b) and 8(c) show the corresponding system fuel cost, net-load profile, and generator dispatch schedule.

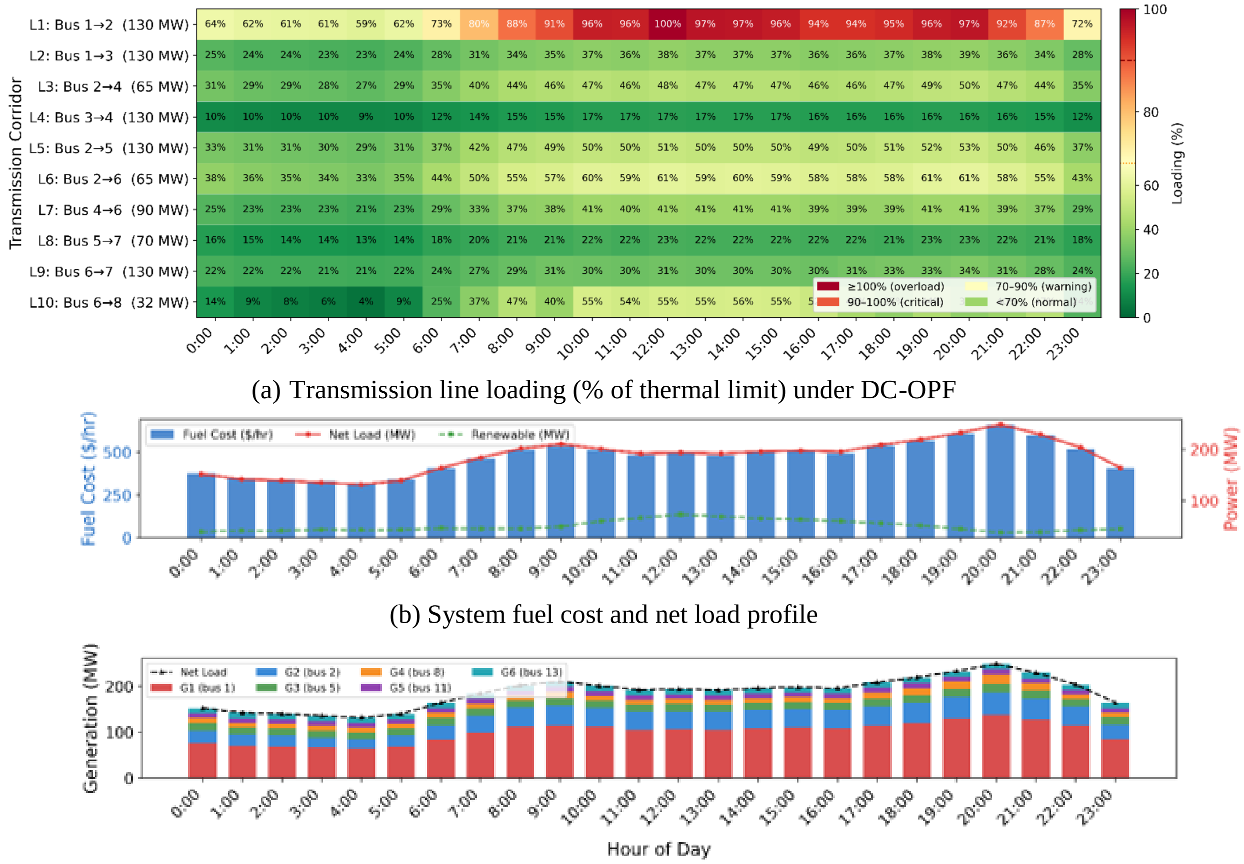

(a) Transmission line loading (% of thermal limit) under DC-OPF

(b) System fuel cost and net load profile

(c) Generator dispatch schedule

Fig. 8 DC-OPF operating results: (a) hourly transmission-line loading expressed as a percentage of thermal rating, (b) system fuel cost and net-load profile, and (c) generator dispatch schedule

The heatmap shows that L1 is the most heavily loaded line and has the highest percentage loading. Importantly, no line exceeds 100% utilization, which confirms that the 30-bus network is not transmission-binding for the generation portfolio studied.

5.6 *Sensitivity, Higher Penetration, and Contingency Screening*

Because the base network is only weakly constrained by transmission limits, the small premium reported previously belongs to that operating point and not to the method in general. To locate the conditions under which it stops holding, the renewable level and the corridor ratings were varied, and every single-line outage was screened. Table 6 and Fig. 9 give the sensitivity, and Fig. 10 gives the contingency screen. Each cell of Table 5 lists the total curtailment in MWh with the congestion premium in brackets.

Table 6 Total curtailment in MWh (congestion premium in brackets) against renewable penetration and corridor rating

Transmission limit / Penetration	1.0x	1.5x	2.0x	2.5x
100% (nominal)	0.0 (0.1%)	10.3 (0.3%)	149.3 (1.8%)	545.7 (5.0%)
70%	0.0 (4.5%)	116.8 (9.7%)	572.3 (22.9%)	1167.8 (35.0%)
55%	44.7 (10.4%)	464.3 (24.6%)	1069.1 (44.4%)	1678.1 (59.2%)
45%	231.6 (19.2%)	828.0 (39.2%)	1437.0 (61.6%)	2046.0 (78.0%)

Two observations emerge from Table 5. At nominal ratings, the curtailment stays at zero until penetration is well above the base level, which confirms spare network capacity in the studied system. Once the corridors are cut to roughly half of their rating, or penetration is doubled, the curtailment climbs into the hundreds of MWh, and the premium passes ten and then twenty per cent. The change is gradual rather than abrupt, which is advantageous for planning purposes.

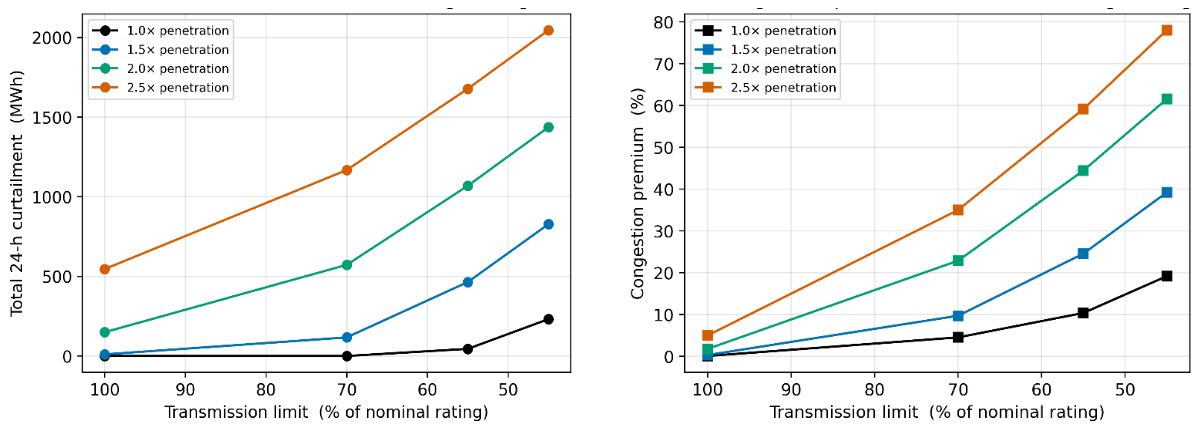

(a) Curtailment vs transmission tightening (b) Congestion premium vs transmission tightening

Fig. 9 Total 24-hour curtailment and congestion premium under different transmission corridor ratings and renewable penetration levels

The contingency screen shown in Fig. 10 was run at nominal penetration with the corridors at seventy per cent of rating. The loss of either of the two corridors that carry power out of the renewable bus, the 1-2 and 1-3 lines, is the most severe: each raises the premium to about twenty per cent, substantially reducing the export capability of renewable generation, and forces close to 240 MWh of curtailment, while the 1-3 outage cannot be served within limits in every hour. The loss of the 6-8 line separates the downstream generators and is reported as a system-separation case rather than as a dispatch result. The remaining outages produce comparatively limited impacts. Raising demand by 15% on the intact network keeps curtailment at zero but lifts the premium to between one and seven per cent, so heavier loading by itself does not create a curtailment problem in this system; the binding factor is corridor capacity relative to renewable injection.

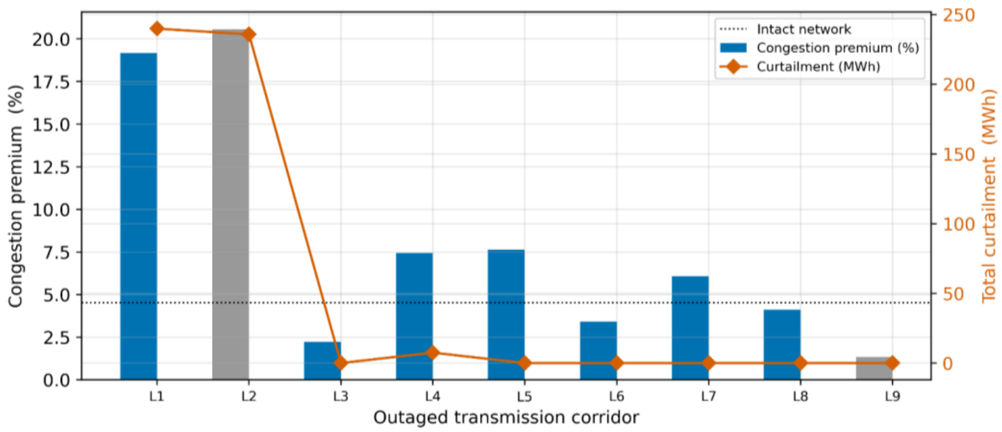

Fig. 10 N-1 contingency screen at nominal penetration and 70% corridor ratings: congestion premium (bars) and curtailment (line) for each outaged corridor

5.7 *Operational Insights for New Energy Management Systems*

The comparison supports four practical observations for source-load dispatch platforms and new energy management systems:

(1) First, transmission-aware dispatch should be treated as a default operational requirement rather than as an optional refinement. In the studied system, DC-OPF preserves near-zero curtailment with only a small cost increase.

(2) Second, multi-objective optimization remains valuable even when the observed cost premium is small. It provides an explicit way to inspect whether the system is operating in a regime with a meaningful cost-curtailment conflict or in a regime where renewable accommodation is readily achievable.

(3) Third, curtailment cannot be interpreted solely as a renewable issue. It is a system flexibility issue shaped by thermal minimum limits, ramping capability, network topology, and the availability of flexible demand or storage.

(4) Fourth, the present framework is extensible to richer formulations that include emissions, reserve procurement, battery state of charge, or demand response participation.

Taken together, the results separate two regimes. In the operating regime represented by the base case, the network has enough headroom that renewable energy is accommodated with negligible economic impact, the cost-curtailment trade-off is weak, and a transmission-aware DC-OPF is both accurate and quick to solve, so a multi-objective metaheuristic adds little, and on this smooth problem even falls a few per cent short on cost. The trade-off only becomes significant when corridor capacity is scarce relative to renewable injection, which is where the sensitivity and contingency results show the premium climbing. For a new-energy management system, the practical signal of curtailment risk is therefore corridor headroom and contingency exposure, rather than the penetration figure on its own. These observations are drawn within the tested scope of one modified IEEE 30-bus system, a deterministic 24-hour profile, and a lossless DC model. Consequently, the weak cost-curtailment trade-off reported here belongs to this regime and is not a general statement about NSGA-II or about multi-objective dispatch as a whole.

6. Conclusion

This study presented and evaluated a transmission-aware source-load dispatch framework based on DC-OPF for balancing operating economy and renewable energy curtailment in modern power systems. The framework was tested on a modified IEEE 30-bus system over a 24-hour scheduling horizon and compared with an unconstrained economic dispatch baseline and an NSGA-II-based multi-objective approach. The comparison was carried out using the same load profile, renewable generation profile, and generator operating constraints in order to assess cost performance, renewable accommodation, and dispatch feasibility under practical operating conditions. The main conclusions are summarized as follows:

(1) The DC-OPF framework achieved a total operating cost of $11,328.51 with only 0.03 MWh of renewable curtailment, showing strong performance in balancing economy and renewable utilization.

(2) Compared with the unconstrained baseline cost of $11,282.26, the DC-OPF solution increased the operating cost by only 0.41%, which indicates that transmission-feasible dispatch can be achieved with a very small economic penalty.

(3) Compared with the NSGA-II solution, which produced a total cost of $11,768.95 and 5.81 MWh of curtailment, the DC-OPF approach provided a more effective operating compromise for the studied system.

(4) The results indicate that, for the modified IEEE 30-bus system under the tested conditions, near-complete renewable energy utilization can be achieved without imposing a significant economic burden.

(5) The study confirms that transmission-aware dispatch is more suitable for practical source-load operation management than unconstrained dispatch when both renewable accommodation and system feasibility must be maintained.

(6) The proposed framework is also suitable for extension to more advanced operational settings, including storage integration, demand response, reserve scheduling, and emission-aware dispatch.

(7) These conclusions are bounded by the tested scope, which uses one modified IEEE 30-bus system, a deterministic 24-hour profile, and a lossless DC model without reactive power or voltage limits. The small-premium result therefore describes this regime rather than a general rule, since the sensitivity and contingency cases show the same network reaching large curtailment and double-digit premiums when the corridors are tightened, or a line is lost. The comparison also does not claim that NSGA-II is weak in general, only that the gradient-based transmission-aware solver suits this smooth, network-light problem better.

(8) Several extensions follow from these limits. The most useful are an AC-OPF check of the premiums; stochastic profiles with a scenario or chance-constrained treatment of wind and solar; the addition of storage, demand response, and reserve procurement as flexibility; unit commitment so that minimum up and down times enter the schedule; and a comparison of

NSGA-II with other population-based methods on the stressed, congested cases where the trade-off is genuinely two-dimensional. Testing the framework on larger systems would also show how the run-time gap between the deterministic and metaheuristic solvers scales.

Nomenclature

Symbol	Description
t, T	index and number of hourly intervals (T = 24 h)
g, G	index and number of thermal generators (G = 6)
1	index of a monitored transmission line
ω	feasible set defined by the operating constraints
$P_{g,t}$	real power output of unit g at hour t (MW)
r_t^u, r_t^c	utilized and curtailed renewable power at hour t (MW)
$\theta_{i,t}$	voltage angle of bus i at hour t (rad)
a_g, b_g, c_g	fuel-cost coefficients of unit g (\$, \$/MWh, and \$/MW^{2}h)
P_g^{min}, P_g^{max}	minimum and maximum output of unit g (MW)
R_g	ramp-rate limit of unit g (MW/h)
D_t	system demand at hour t (MW)
R_t^a	available renewable power at hour t (MW)
x_l, F_l^{max}	reactance (p.u.) and thermal limit (MW) of line l
B	reduced nodal susceptance matrix
C, C_T	total 24-h operating cost (\$) and total curtailment (MWh)
$v(x)$	aggregate constraint-violation measure
DC-OPF	DC optimal power flow
NSGA-II	non-dominated sorting genetic algorithm II
SBX, PM	simulated binary crossover, polynomial mutation
SLSQP	sequential least-squares quadratic programming

Appendix: Case-Study Data

This appendix lists the data required to reproduce the case study.

Table A1 Distribution of system demand across the active buses

Bus	Share of system demand (%)
1 (reference / renewable)	0
2	12
3	10
4	6
5	25
6	7
7	21
8	19

Table A2 Hourly load and renewable availability used in the case study

Hour (h)	Load (MW)	Solar (MW)	Wind (MW)	Net load (MW)
0	191.99	0.0	39.73	152.26
1	183.62	0.0	41.45	142.17
2	181.30	0.0	41.48	139.81
3	179.35	0.0	43.82	135.53
4	174.71	0.0	43.08	131.63
5	183.21	0.0	43.55	139.67
6	210.76	3.76	43.12	163.89
7	229.98	7.86	37.8	184.32

Table A2 Hourly load and renewable availability used in the case study (continued)

Hour (h)	Load (MW)	Solar (MW)	Wind (MW)	Net load (MW)
8	247.40	12.98	32.65	201.76
9	260.20	19.61	29.89	210.7
10	261.59	28.96	31.6	201.03
11	258.75	34.01	32.52	192.22
12	267.42	39.7	33.5	194.23
13	261.10	37.13	31.97	192.0
14	261.90	33.89	32.02	195.99
15	261.17	28.43	34.82	197.92
16	256.42	20.7	39.96	195.76
17	264.90	13.05	42.95	208.89
18	271.04	7.42	44.46	219.15
19	277.40	3.79	41.07	232.54
20	286.80	0.0	38.35	248.44
21	268.27	0.0	39.12	229.15
22	246.85	0.0	42.81	204.04
23	209.33	0.0	45.04	164.29

Conflicts of Interest

The authors declare no conflict of interest.

References

[1] H.-Q. Deng, H. Wu, Z.-W. Liang, P.-R. Zheng, and J.-F. Shen, "Proactive Prevention Strategies for Grid Risk Scenarios Based on Pumped Storage Participation," International Journal of Engineering and Technology Innovation, vol. 14, no. 4, pp. 389-406, 2024.

[2] M. M. Rahman, S. H. Dadon, M. He, M. Giesselmann, and M. M. Hasan, "An Overview of Power System Flexibility: High Renewable Energy Penetration Scenarios," Energies, vol. 17, no. 24, article no. 6393, 2024.

[3] Y. Sharifian and H. Abdi, "Multi-Area Economic Dispatch Problem: Methods, Uncertainties, and Future Directions," Renewable and Sustainable Energy Reviews, vol. 191, article no. 114093, 2024.

[4] G. Papazoglou and P. Biskas, "Review and Comparison of Genetic Algorithm and Particle Swarm Optimization in the Optimal Power Flow Problem," Energies, vol. 16, no. 3, article no. 1152, 2023.

[5] S. Park and P. Van Hentenryck, "Self-Supervised Learning for Large-Scale Preventive Security Constrained DC Optimal Power Flow," IEEE Transactions on Power Systems, vol. 40, no. 3, pp. 2205-2216, 2024.

[6] B. Taheri and D. K. Molzahn, "Optimizing Parameters of the DC Power Flow," Electric Power Systems Research, vol. 235, article no. 110719, 2024.

[7] M. A. Abido, "Multiobjective Evolutionary Algorithms for Electric Power Dispatch Problem," IEEE Transactions on Evolutionary Computation, vol. 10, no. 3, pp. 315-329, 2006.

[8] H. Nourianfar and H. Abdi, "Environmental/Economic Dispatch Using a New Hybridizing Algorithm Integrated with an Effective Constraint Handling Technique," Sustainability, vol. 14, no. 6, article no. 3173, 2022.

[9] H. Y. Shahri, S. A. Hosseini, and J. Pourhossein, "Multi-Objective Evolutionary Method for Multi-Area Dynamic Emission/Economic Dispatch Considering Energy Storage and Renewable Energy Units," Heliyon, vol. 10, no. 18, article no. e37476, 2024.

[10] D. Zou, L. Ma, and C. Li, "An Enhanced NSGA-II and a Fast Constraint Repairing Method for Combined Heat and Power Dynamic Economic Emission Dispatch," Information Sciences, vol. 678, article no. 120915, 2024.

[11] S. Bhavsar, R. Pitchumani, J. Maack, I. Satkauskas, M. Reynolds, and W. Jones, "Stochastic Economic Dispatch of Wind Power under Uncertainty Using Clustering-Based Extreme Scenarios," Electric Power Systems Research, vol. 229, article no. 110158, 2024.

[12] A. Ali, G. Abbas, M. U. Keerio, M. A. Koondhar, K. Chandni, and S. Mirsaeidi, "Solution of Constrained Mixed-Integer Multi-Objective Optimal Power Flow Problem Considering the Hybrid Multi-Objective Evolutionary Algorithm," IET Generation, Transmission & Distribution, vol. 17, no. 1, pp. 66-90, 2023.

[13] S. Li, W. Gong, L. Wang, and Q. Gu, "Multi-Objective Optimal Power Flow with Stochastic Wind and Solar Power," Applied Soft Computing, vol. 114, article no. 108045, 2022.

[14] A. Maheshwari, Y. R. Sood, and S. Jaiswal, “Flow Direction Algorithm-Based Optimal Power Flow Analysis in the Presence of Stochastic Renewable Energy Sources,” Electric Power Systems Research, vol. 216, article no. 109087, 2023.

[15] L. Bird, D. Lew, M. Milligan, E. M. Carlini, A. Estanqueiro, D. Flynn, et al., “Wind and Solar Energy Curtailment: A Review of International Experience,” Renewable and Sustainable Energy Reviews, vol. 65, pp. 577-586, 2016.

[16] P. Pijarski, C. Saigustia, P. Kacejko, A. Belowski, and P. Miller, “Optimal Network Reconfiguration and Power Curtailment of Renewable Energy Sources to Eliminate Overloads of Power Lines,” Energies, vol. 17, no. 12, article no. 2965, 2024.

[17] M. Laimon, “Renewable Energy Curtailment: A Problem or an Opportunity?,” Results in Engineering, vol. 26, article no. 104925, 2025.

[18] L. Ren, D. Peng, D. Wang, J. Li, and H. Zhao, “Multi-Objective Optimal Dispatching of Virtual Power Plants Considering Source-Load Uncertainty in V2g Mode,” Frontiers in Energy Research, vol. 10, article no. 983743, 2023.

[19] J. Li, J. Guo, and Y. Deng, “Multi-Objective Optimization for Economic Load Distribution and Emission Reduction with Wind Energy Integration,” International Journal of Electrical Power & Energy Systems, vol. 161, article no. 110175, 2024.

[20] J. Nie, L. Zhou, M. F. Kaye, C. C. Silveira, A. Nwokolo, X. Jiang, et al., “High-Performance Optimal Power Flow Estimation for EV-Interfaced Microgrids with Standardized Grid Services,” IEEE Transactions on Industry Applications, vol. 59, no. 1, pp. 1199-1211, 2022.

[21] M. Abid, M. Belazzoug, S. Mouassa, A. Chanane, and F. Jurado, “Multi-Objective Optimal Power Flow Analysis Incorporating Renewable Energy Sources and Facts Devices Using Non-Dominated Sorting Kepler Optimization Algorithm,” Sustainability, vol. 16, no. 21, article no. 9599, 2024.

[22] K. Deb, A. Pratap, S. Agarwal, and T. Meyarivan, “A Fast and Elitist Multiobjective Genetic Algorithm: NSGA-II,” IEEE Transactions on Evolutionary Computation, vol. 6, no. 2, pp. 182-197, 2002.

[23] P. P. Biswas, P. N. Suganthan, R. Mallipeddi, and G. A. J. Amaratunga, “Multi-Objective Optimal Power Flow Solutions Using a Constraint Handling Technique of Evolutionary Algorithms,” Soft Computing, vol. 24, no. 4, pp. 2999-3023, 2020.

[24] Z. Wang, A. Younesi, M. V. Liu, G. C. Guo, and C. L. Anderson, “AC Optimal Power Flow in Power Systems with Renewable Energy Integration: A Review of Formulations and Case Studies,” IEEE Access, vol. 11, pp. 102681-102712, 2023.

[25] M. M.-U.-T. Chowdhury, K. Murari, M. S. Hasan, and S. Kamalasadan, “Optimal Power Flow (OPF) Analysis for AC–DC Active Distribution Networks Utilizing Second-Order Cone Programming (SOCP) Approach,” IEEE Transactions on Industrial Informatics, vol. 21, no. 5, pp. 3555-3564, 2025.

[26] E. Obio, S. Ali, I. Oyebanjo, D. Abara, F. Suleiman, P. Ohiero, et al., “Comparison of Economic Dispatch, OPF and Security Constrained-OPF in Power System Studies R^N,” Journal of Power and Energy Engineering, vol. 10, no. 8, pp. 54-74, 2022.

[27] S. A. Mohamed, N. Anwer, and M. M. Mahmoud, “Solving Optimal Power Flow Problem for IEEE-30 Bus System Using a Developed Particle Swarm Optimization Method: Towards Fuel Cost Minimization,” International Journal of Modelling and Simulation, vol. 45, no. 1, pp. 307-320, 2025.